Acta Mech 235, 285–301 (2024)
https://doi.org/10.1007/s00707-023-03752-7

ORIGINAL PAPER

Nagesh Dhore · Lalsingh Khalsa · Vinod Varghese

Transient hygrothermoelastic damping analysis of cylindrical nanobeams within a fractional order system

Received: 14 July 2023 / Revised: 15 September 2023 / Accepted: 23 September 2023 / Published online: 21 October 2023

Abstract The interactions between temperature and moisture's impacts on structural instability are relatively significant in environments with high heat and humidity levels. This study uses a fractional order framework to build a coupled hygrothermoelastic model with non-Fick and non-Fourier effects by taking into account two temperatures, conductive and thermodynamic heat flow. The hygrothermoelastic damping behavior of the cylindrical nanobeams is modeled using the Euler–Bernoulli beam theory, and an explicit solution is obtained using Laplace transform and mode analysis. The inverse Laplace transforms are computed numerically using a method based on Fourier expansion techniques. The numerical results for various aspect ratios and end supports are examined. The effects of the temperature discrepancy factor due to heat flow on the damping and frequency shift within the hygrothermoelastic nano-cylindrical beam are illustrated graphically. The numerical findings show that moisture availability increases the damping of the nanoscale beam, resulting in increased energy dissipation.

1 Introduction

Classical continuum theory is size-independent and cannot provide a good prediction for small scales. Thus, the size-dependent continuum theories, such as the strain gradient theory, couple stress theory, micropolar theory, nonlocal elasticity theory, were developed to characterize the size-dependent effect in the nanostructures by introducing an intrinsic length scale. MEMS/NEMS devices have high sensitivity as well as fast response. It is necessary to know how the parameters affect their physical properties and mechanical properties. Unfortunately, it has been consistently observed that energy dissipation increases with size decreasing significantly. It has been verified that thermoelastic damping is a significant loss mechanism near room temperature in MEMS/NEMS devices. The complex relationship between heat, moisture, and deformation poses various engineering challenges with significant real-world implications. The transient nature of the boundary circumstances will determine the degree to which these consequences are linked. They may, therefore, be used to predict considerable coupling effects as boundary conditions change in circumstances where coupling effects are relatively insignificant by obtaining them from current experimental data. This can be done in cases where the coupling effects are relatively small. It makes it feasible to investigate with a greater degree of precision

N. Dhore (✉)
Department of Mathematics, Gramgeeta Mahavidyalaya Chimur, Chandrapur, India
e-mail: nageshdhore@gmail.com

N. Dhore · L. Khalsa · V. Varghese
Department of Mathematics, M. G. College, Armori, Gadchiroli, India
e-mail: lalsinghkhalsa@yahoo.com

V. Varghese
e-mail: vino7997@gmail.com

understanding how a substance reacts to severe climatic circumstances. It is common for there to be a shortage of such expertise, which presents a significant barrier to the creation of new technology advancements [1].

To investigate the constitutive relationships between temperature, moisture content, and deformation in porous materials [2], a straightforward linear hygrothermoelastic model has been derived and then transformed into a single fourth-order ordinary differential equation by the application of the Laplace transformation. To evaluate hygrothermoelastic stress in composite laminating plates throughout moisture desorption, Benkhedda et al. [3] evaluated an approximation model while taking into account a change in mechanical characteristics brought on by temperature and moisture variations. Based on a higher-order shear deformation theory, Nguyen et al. [4] studied the hygrothermal impacts on vibration and buckling analysis of functionally graded beams. This theory explains the higher-order variation of in-plane and out-of-plane displacements as well as the hyperbolic distribution of transverse shear stress. The Ritz solution method is used to solve problems with different boundary conditions. Zenkour [5] examined into the hygrothermomechanically induced bending of a thin, variable-thickness rectangular plate with two of the plate's opposite edges clamped and the other two simply supported. By utilizing von Kármán geometric nonlinearity and the Euler–Bernoulli theory, Tang and Ding [6] presented a study of the nonlinear hygrothermal dynamics of a bidirectionally functionally graded beam with linked transverse and longitudinal displacements. In their paper [7], for a non-simple material that is rigid in both classical Fourier's and Fick's laws, the author developed a new model of two-temperature hygrothermoelastic diffusion theory that results in a multilayered elliptic plate that is perpendicular to the axis when subjected to hygrothermal load. Jan et al. [8] conducted an experimental method for analyzing the performance of an externally actuated Complementary Metal–Oxide–Semiconductor (CMOS)—MEMS paddle resonator under the effect of varying temperature and humidity environment using Field Emission Scanning Electron Microscopy (FESEM). Eichler et al. [9] examined the damping of mechanical resonators and tested them in a variety of objects, including the Foucault pendulum, carbon nanotubes, and graphene sheets. Ebrahimi and Barati [10] investigated the effects of temperature rise, moisture concentration rise, length scale parameter, elastic foundation, nonlocal parameter, and geometrical parameters on a nonlocal strain gradient plate model on elastic substrate derived via Hamilton's principle for buckling study of graphene sheets in hygrothermal environments. Most of these studies are founded on Fourier and Fick's laws, a well-known and commonly applied classical principle in the hygrothermoelastic theory. On the other hand, Fourier and Fick's classical form has a significant law in assuming an infinitely fast propagation. The Fourier and Fick model has been improved by introducing a given characteristic time constant, known as phase lag of the heat flux or so-called relaxation time, to remove the paradox of infinite speed propagation. With the Introduction of single-phase lag to evade the discrepancy between the mathematical model and the experimental observations, this extension turns the parabolic into a hyperbolic equation.

Based on the above assumption, different models were suggested by various authors. Some generalized diffusion or heat conduction models have been presented to address this, including the hyperbolic heat conduction model [11], the dual-phase-lag diffusion model [12], and the fractional diffusion models [13]. Sun et al. [14] investigated the generalized thermoelastic theory with one relaxation period by utilizing the finite sine Fourier transformation approach with the Laplace transformation and the normal mode analysis for the damping of micro-scale beam resonators that were impacted by pulsed lasers. Kakhki et al. [15] presented an analytical method for studying Thermo-Elastic Damping (TED) and the dynamic behavior of microbeam resonators as MEMS and solved it analytically by employing the Laplace transform techniques for spatial variables. Youssef et al. [16] studied the thermal analysis of the thermal quality factor set for a silicon microbeam resonator subjected to static prestress. The solutions based on the Lord–Shulman and dual-phase-lag heat conduction models with fractional derivatives are obtained in six different heat conduction models.

The entire body of work that has been done up until this point has investigated chiefly the thermoelastic effects in MEMS with dimensions typically ranging from tens to hundreds of micrometers. Despite this, there are considerable benefits that may be gained from MEMS by decreasing their size and switching to different materials. Devices with dimensions on the nanoscale are often referred to as NEMS, and they tend to operate at higher frequencies while consuming less power than MEMS devices. NEMS has the potential to integrate more smoothly and provide unique functionalities [17]. Elsibai and Youssef [18] investigated how the relationship between temperature and strain rate became dominant within the nanoscale beam and came up with a general solution for the vibration of a gold nanobeam resonator brought on by ramp heating in the context of the Green and Naghdi model of generalized thermoelasticity. Zhou and Li [19] investigated the Heat-Conduction Dimension (HCD) utilizing micro/nano-ring resonators with a rectangular cross section and the Dual-Phase-Lagging (DPL) non-Fourier theory. By combining the Euler–Bernoulli beam theory with Lord and Shulman's theory of generalized thermoelasticity and memory-dependent heat conduction, Wang et al. [20] explored the

thermoelastic damping in a microbeam with a rectangular cross-section. Using the theory of 'non-Fickian' mass diffusion, Shaw and Othman [21] examined the thermodynamic damping on mass diffusion in the solid body deformation induced by heat coming from a cavity into the medium caused by heat coming from a cavity into the medium.

There have not been a lot of studies completed in this field based on generalized diffusion theories, which is noteworthy when it comes to hygrothermoelastic challenges. The generalized magneto-thermoelasticity equations were developed by Ezzat et al. [22] in two dimensions with two relaxation times, and they were solved using the matrix exponential method, which is the cornerstone of the state space approach used in modern theory. El-Karamany and Ezzat [23] obtained a novel generalized thermoelasticity theory with two-time delays and kernel functions. With this theory, the constitutive equations for the thermoelastic diffusion in anisotropic and isotropic solids are constructed, which results in the linked thermoelastic diffusion and Lord–Shulman theories as special instances. Hosseini et al. [24] performed an investigation with the use of local integral equations for coupled two-dimensional (2D) non-Fick hygrothermoelasticity analysis made on the Meshless Petrov–Galerkin (MLPG) technique. Peng et al. [25] developed a non-Fourier hyperbolic temperature-moisture coupling model for convective surfaces. This model takes into account the Dufour effect as well as the Soret effect and is based on the phase delay of heat and moisture fluxes. Convective surfaces were used in the construction of this model. Xue et al. [26] proposed a hyperbolic hygrothermal coupled model to explore the fracture problem of a hollow cylinder with a circumferential crack by extending the traditional laws of heat conduction and diffusion formulated by Fourier and Fick's law, respectively. A time-fractional coupled hygrothermal theory was developed by Zhang and Li [27–29] to explain the inconsistent phenomenon of coupled hygrothermal diffusion and to obtain the solution using the integral transform approach. Later, they introduced relaxation times or phase lags of heat flux and moisture flux via mode analysis to get a coupled hygrothermoelastic model.

The earlier research studies indicated that the non-Fourier of hygrothermal diffusion coupling is both evident and essential; these effects cannot be ignored. This is incredibly accurate when referring to coupled hygrothermoelastic medium. This paper investigates the hygrothermal coupling effects of a nanoscale cylindrical beam's damping and frequency shifts. A novel non-simple hygrothermoelastic model that considers temperature discrepancy factors has been developed to represent the coupling behaviors of heat, moisture, and elastic deformations. One may, therefore, obtain the explicit formulas for hygrothermoelastic damping using this information. The consequences of coupled hygrothermoelastic and generalized diffusion parameters on the inverse quality factor are discussed with the help of the following illustration and the graphical depiction that follows it.

2 The formulation for the hygrothermal equation for non-simple medium

We first propose a theory of time-fractional hygrothermoelasticity for a non-simple medium in this paper. In order to maintain simplicity, it is considered that heat and moisture are coupled and that both have an impact on the elastic stresses in the medium. As a consequence, the interaction between heat and moisture can be characterized as water vapor diffusion through a material's pores, which are partially filled with solids and air. In general, according to [30], the amount of moisture absorbed by a unit mass of a solid M, can be assumed to depend linearly on the concentration of water vapor contained in a unit volume of void C, and the temperature T, and change in moisture and temperature is confined within a small range; the amount of moisture absorbed by a unit mass of a solid is given by,

$$M = \chi C - \omega T + \text{constant} \tag{1}$$

where χ and ω are material constants. Then, the amount of moisture contained in the composite per unit mass of solid m can be written as,

$$m = \nu' C/\rho + M \tag{2}$$

where ν' is the volume fraction of the voids, and ρ is the density of the material, defined as $\rho = \left(1 - \nu'\right)\rho_{\mathrm{s}}$, with ρ_s being the density of the solid without voids.

Due to the principles of energy conservation and mass conservation, taking into account the volume strain $-z\,(\partial^2 w/\partial r^2)$, we can write

$$\nabla \cdot q_h = \rho\gamma \frac{\partial M}{\partial t} - \rho c_p \frac{\partial T}{\partial t} + E\alpha_1\alpha_2 T_0 \frac{\partial}{\partial t}\left(z\frac{\partial^2 w}{\partial r^2}\right), \tag{3}$$

$$\nabla \cdot q_m = -\frac{\rho}{\nu'}\frac{\partial M}{\partial t} - \frac{\partial C}{\partial t}, \tag{4}$$

where α_1, α_2 are the coefficients of linear thermal expansion and moisture absorption, q_{h} is the heat flux vector and q_{m} is the moisture flux vector, γ is the amount of heat released per unit mass of moisture, c_{p} is the specific heat at constant pressure, and w is often called the transverse deflection of the cylindrical beam, respectively.

Following [31], heat and moisture are assumed to obey time-fractional Fourier and Fick's laws where the matter flux has the power time-nonlocal kernel describing "long-tail" memory. Thus, the heat flux vector q_{h} and moisture flux vector q_{m} take the following forms:

$$q_{\mathrm{h}}(t) = \begin{cases} -\frac{D_h}{\Gamma(\alpha)}\frac{\partial}{\partial t}\int_0^t (t-\tau)^{\alpha-1}\nabla T(\tau)\mathrm{d}\tau, & 0 < \alpha \le 1, \\ -\frac{D_h}{\Gamma(\alpha-1)}\int_0^t (t-\tau)^{\alpha-2}\nabla T(\tau)\mathrm{d}\tau, & 1 < \alpha \le 2, \end{cases} \tag{5}$$

$$q_{\mathrm{m}}(t) = \begin{cases} -\frac{D_m}{\Gamma(\beta)}\frac{\partial}{\partial t}\int_0^t (t-\tau)^{\beta-1}\nabla C(\tau)\mathrm{d}\tau & 0 < \beta \le 1, \\ -\frac{Dm}{\Gamma(\beta-1)}\int_0^t (t-\tau)^{\beta-2}\nabla C(\tau)\mathrm{d}\tau & 1 < \beta \le 2, \end{cases} \tag{6}$$

in which α, β are the fractional orders, and $\Gamma(*)$ is the Gamma function.

Putting Eqs. (5) and (6) into Eqs. (3) and (4), we get

$$D_h\nabla^2 T = -\rho\gamma\frac{\partial^\alpha M}{\partial t^\alpha} + \rho c_p\frac{\partial^a T}{\partial t^\alpha} - E\alpha_1\alpha_2 T_0\frac{\partial^\alpha}{\partial t^\alpha}\left(z\frac{\partial^2 w}{\partial r^2}\right), 0 < \alpha \le 2, \tag{7}$$

$$D_m\nabla^2 C = \frac{\rho}{\nu'}\frac{\partial^\beta M}{\partial t^\beta} + \frac{\partial^\beta C}{\partial t^\beta}, 0 < \beta \le 2, \tag{8}$$

in which $(\partial^\alpha/\partial t^\alpha)$ and $\left(\partial^\beta/\partial t^\beta\right)$ are the Caputo fractional derivatives [32] as

$$\frac{\mathrm{d}^\alpha f(t)}{\mathrm{d}t^\alpha} = \begin{cases} \frac{1}{\Gamma(n-\alpha)}\int_0^t (t-\tau)^{n-\alpha-1}\frac{\mathrm{d}^n f(\tau)}{\mathrm{d}\tau^n}\mathrm{d}\tau, & n-1 < \alpha < n \\ \frac{\mathrm{d}^n f(\tau)}{\mathrm{d}t^n}, & \alpha = n \end{cases} \tag{9}$$

The quantity M in Eqs. (7) and (8) can be eliminated using Eq. (1); we get the system of linearly coupled partial differential equation of moisture (C) and temperature (T) as follows,

$$\mathfrak{D}\nabla^2 T = \frac{\partial^\alpha}{\partial t^\alpha}\left[T - \eta C - \frac{E\alpha_1\alpha_2 T_0}{\rho(\gamma\omega + c_p)}z\frac{\partial^2 w}{\partial r^2}\right], 0 < \alpha \le 2, \tag{10}$$

$$D\,\nabla^2 C = \frac{\partial^\beta}{\partial t^\beta}(C - \lambda T), 0 < \beta \le 2 \tag{11}$$

where ∇^2 is the Laplacian operator involving two variable parameters, η is the adiabatic coefficient, λ is an isothermal coefficient, $\mathfrak{D}$ and D are thermal diffusion coefficient under the state of constant vapor concentration and vapor diffusion coefficient under isothermal condition, respectively, and it is represented as

$$\mathfrak{D} = \frac{D_h}{\rho(c_p + \gamma\omega)}, \eta = \frac{\gamma\chi}{c_p + \gamma\omega}, \tag{12}$$

$$D = \frac{D_m\nu'}{\nu' + \rho\chi}, \lambda = \frac{\rho\omega}{\nu' + \rho\chi}, \tag{13}$$

The two-temperature model is a non-classical thermoelasticity theory of elastic solids currently being introduced. In this context [33, 34], it recommended separating real materials into simple and non-simple materials by taking into account two temperatures (conductive and thermodynamic), and they have shown that the two temperatures are related by,

$$\phi = T - b\,\nabla^2 T\,,\ b > 0 \tag{14}$$

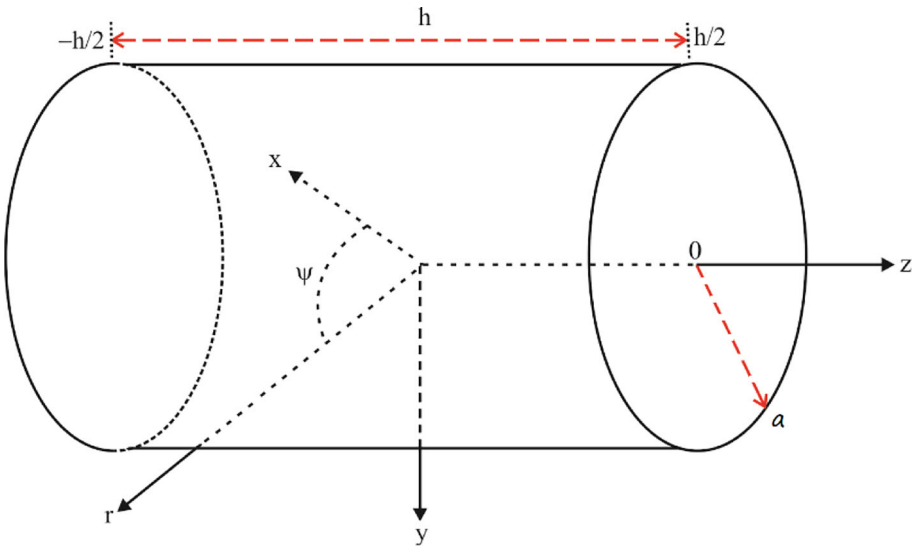

Fig. 1 Cross-sectional configuration of a cylindrical beam

in which ϕ is the thermodynamic temperature, T is the conductive temperature, and b is the temperature discrepancy factor. Because of this, the thermodynamics and conductivity temperatures are the same for simple materials but not for non-simple materials.

The parameter b is a crucial distinction between the two-temperature thermoelasticity and classical theories. Specifically, in the limit which gives rise to the classical theory, i.e., one temperature generalized thermoelasticity theory. Therefore, for a non-simple medium, Eq. (10) can be written as,

$$\mathfrak{D}\left(1+\frac{b}{\kappa}\frac{\partial}{\partial t}\right)\nabla^2 T=\frac{\partial^{\alpha}}{\partial t^{\alpha}}\left[T-\eta C-\frac{E\alpha_1\alpha_2 T_0 z}{\rho(c_p+\gamma\omega)}\frac{\partial^2 w}{\partial r^2}\right],\ 0<\alpha\leq 2. \tag{15}$$

Therefore, the system of linearly coupled partial differential equations is represented by Eqs. (11) and (15).

3 Formulation of the problem

To investigate the vibration of an Euler–Bernoulli cylindrical beam with circular cross sections subjected to hygrothermal loadings at the surface, as illustrated in Fig. 1, the cylindrical coordinates system $(r,\ \psi,\ z)$ is utilized.

Take a look at the small flexural deflections of a cylindrical beam with z-axes specified along the longitudinal with length $z\ (-h/2\leq z\leq h/2)$, width radius $r\ (0\leq r\leq a)$, and $\psi\ (0\leq\psi\leq 2\pi)$. When the cylindrical beam is unstretched, unstrained, and has no damping mechanism when the cylinder is at rest, and the temperature is T_0, moisture is C_0 everywhere. Due to the symmetry of this problem, the coupled partial differential equation for a non-simple material is represented by the system of differential Equations where temperature and moisture are finite in the cylindrical beam for any time. Hence, we can write

$$\mathfrak{D}\left(1+\frac{b}{\kappa}\frac{\partial}{\partial t}\right)\nabla^2 T=\frac{\partial^{\alpha}}{\partial t^{\alpha}}\left(T-\eta C-\frac{z\alpha_2\Delta_E}{\alpha_1}\frac{\partial^2 w}{\partial r^2}\right),\ 0<\alpha\leq 2 \tag{16}$$

$$D\,\nabla^2 C=\frac{\partial^{\beta}}{\partial t^{\beta}}(C-\lambda T),\ 0<\beta\leq 2 \tag{17}$$

subjected to the initial conditions

$$T(r,0)=T_0\ \text{ and }\ C(r,0)=C_0,\ \text{ for } 0<r<a, \tag{18}$$

$$\begin{aligned}\frac{\partial^{\alpha} T(r,0)}{\partial t^{\alpha}} &= 0\,, \text{ for } 0 < r < a, \text{ if } 1 < \alpha \leq 2,\\ \frac{\partial^{\beta} C(r,0)}{\partial t^{\beta}} &= 0\,, \text{ for } 0 < r < a, \text{ if } 1 < \beta \leq 2,\end{aligned} \tag{19}$$

where

$$\Delta_E = \frac{E\alpha_1^2 T_0}{\rho(c_{\mathrm{p}} + \gamma\omega)}. \tag{20}$$

If $\gamma\omega$ vanishes, Δ_E represents the relaxation strength of the Youngs modulus called as Zener modulus [35], and if $\alpha_2 = 0$, the above system reduces to an uncoupled diffusion equation of hygrothermoelastic temperature, moisture, and displacement distribution. The above system reduces to a coupled diffusion equation of hygrothermoelastic temperature, moisture, and displacement distribution for $\alpha_2 = 1$. We will further discuss the fractional order hygrothermoelastic vibration of a cylindrical beam for both uncoupled and coupled cases.

The cylinder's upper and lower surfaces are assumed to have no heat or moisture flow, equivalent to a vanishing temperature and moisture gradient on both surfaces for this research.

$$\frac{\partial T}{\partial z} = \frac{\partial C}{\partial z} = 0\,,\ z = \pm\frac{h}{2},\ t > 0 \tag{21}$$

Under the Euler–Bernoulli hypothesis, the displacement component is expressed as

$$u_r = -z\frac{\partial w(r,t)}{\partial r}, u_{\psi} = 0,\ u_z(r,t) = w(r,t) \tag{22}$$

For the present investigation, the Euler–Bernoulli beam theory is applied to simulate the thermally induced lateral vibration [36]. The differential equation of the beam's thermally generated lateral vibration may be written as follows:

$$\nabla_1^4 w + \nabla_1^2 M_T + \frac{\rho A}{EI}\frac{\partial^2 w}{\partial t^2} = 0 \tag{23}$$

with conditions

$$w(r,0) = 0,\ \frac{\partial w(r,0)}{\partial t} = 0,\ 0 < r < a \tag{24}$$

where ∇_1 is the Laplace operator involving one variable parameter, ρ is the density of the beam $A = \pi a^2$ is the cross section area, E is Young's modulus, $I = \pi a^4/2$ is the moment of inertia about the z-axis, and $M_T(r, t)$ is the hygrothermal moment given by

$$M_T = \frac{12}{h^3}\int_{-h/2}^{h/2} [\beta_1(T - T_0) + \beta_2(C - C_0]z\,\mathrm{d}z \tag{25}$$

where β_1 is the thermal expansion coefficient and β_2 the moisture absorption coefficient, respectively.

4 Solution of the problem

To solve Eqs. (16) and (17) under appropriate boundary conditions, we introduce the following dimensionless quantities:

$$\begin{aligned}&\hat{w} = w/a,\ \hat{z} = z/a,\ \hat{r} = r/a,\ \hat{h} = h/a,\ (\hat{t}, \hat{b}) = (c/a)\,(t, b),\\ &c = \sqrt{E/\rho},\ \theta = (T - T_0)/T_0,\ \Psi = (C - C_0)/\lambda T_0,\end{aligned} \tag{26}$$

4.1 The coupled case

Then, Eq. (16) and (17) reduces to

$$D_1\left(1+\frac{b}{\kappa}\frac{\partial}{\partial t}\right)\nabla^2\theta=\frac{\partial^\alpha}{\partial t^\alpha}\left(\theta-\eta\lambda\psi-\frac{z\,a\,\alpha_2\Delta_E}{\alpha_1 T_0}\frac{\partial^2 w}{\partial r^2}\right) \tag{27}$$

$$D_2\nabla^2\psi=\frac{\partial^\beta}{\partial t^\beta}(\psi-\theta) \tag{28}$$

where

$$D_1=\frac{\mathfrak{D}a^{\alpha-2}}{c^\alpha},\ D_2=\frac{Da^{\beta-2}}{c^\beta},\ \nabla^2=\frac{\partial^2}{\partial r^2}+\frac{1}{r}\frac{\partial}{\partial r}+\frac{\partial^2}{\partial z^2}. \tag{29}$$

and we have canceled the prime for convenience.

Laplace transform of a real-valued function $f(t),\ t\geq 0$ defined as

$$\overline{f}(s)=L[f(t)]=\int_0^\infty f(t)e^{-st}\mathrm{d}t,\ s>0 \tag{30}$$

where we shall assume that $f(t)$ is piecewise continuous and s is the Laplace parameter.

Apply Laplace transform to Eqs. (27) and (28), we get

$$D_1\left(1+\frac{b}{\kappa}s\right)\nabla^2\overline{\theta}=s^\alpha\left(\overline{\theta}-\eta\lambda\overline{\Psi}-\frac{za\alpha_2\Delta_E}{\alpha_1 T_0}\frac{\partial^2\overline{w}}{\partial r^2}\right) \tag{31}$$

$$D_2\nabla^2\overline{\Psi}=s^\beta(\overline{\Psi}-\overline{\theta}) \tag{32}$$

For the coupled case, to solve the coupled governing Eqs. (31) and (32), the dimensionless temperature and moisture are expressible in terms of an auxiliary function F as follows:

$$\overline{\theta}=\left(D_2\nabla^2-s^\beta\right)\overline{F} \tag{33}$$

$$\overline{\Psi}=-s^\beta\overline{F} \tag{34}$$

It is straightforward to establish that Eqs. (31) and (32) are automatically fulfilled if the previously unknown function F satisfies the equation presented in the following sentence.

$$\begin{aligned}&D_1D_2\left(1+\frac{b}{\kappa}s\right)\nabla^4\overline{F}-\left(D_1s^\beta+D_2s^\alpha+\frac{bD_1s^{1+\beta}}{\kappa}\right)\nabla^2\overline{F}\\&+(1-\eta\lambda)s^{\alpha+\beta}\overline{F}+\frac{z\,a\,\alpha_2\Delta_E}{\alpha_1 T_0}s^\alpha\frac{\partial^2\overline{w}}{\partial r^2}=0\end{aligned} \tag{35}$$

Using the following parameters, we set up a model to determine the effect of hygrothermoelastic damping, on the time-harmonic vibrations in the Laplace domain as

$$(\overline{w},\overline{\theta},\overline{\Psi},\overline{F})=(\overline{w}^*,\overline{\theta}^*,\overline{\Psi}^*,\overline{F}^*)\,e^{i\,\Omega\,s} \tag{36}$$

where Ω is the dimensionless frequency of the beam, and we expect to find that, in most cases, the frequencies are complex, with the imaginary component $|\mathrm{Im}(\Omega)|$ representing the vibration's attenuation and the real part $\mathrm{Re}(\Omega)$ providing the beam's new eigenfrequencies in the presence of thermoelastic coupling.

Substituting Eqs. (36) in (35), one obtains

$$\begin{aligned}&D_1D_2\left(1+\frac{b}{\kappa}s\right)\nabla^4\overline{F}^*-\left(D_1s^\beta+D_2s^\alpha+\frac{bD_1s^{1+\beta}}{\kappa}\right)\nabla^2\overline{F}^*\\&+(1-\eta\lambda)s^{\alpha+\beta}\overline{F}^*+\frac{z\,a\,\alpha_2\Delta_E}{\alpha_1 T_0}s^\alpha\frac{\partial^2\overline{w}^*}{\partial r^2}=0\end{aligned} \tag{37}$$

Note that there are no thermal gradients in the direction and that thermal gradients in the plane of the cross section along the direction are significantly larger than gradients along the beam axis. We neglect the terms $\partial^2/\partial r^2$ and $\partial/\partial r$, replace ∇^2 by $\partial^2/\partial z^2$ [35]. Then, the general solution of Eq. (37) is given by

$$\begin{aligned}\overline{F}^* &= A_1 \sin(k_1 z) + A_2 \cos(k_1 z) + A_3 \sin(k_2 z) + A_4 \cos(k_2 z) \\ &\quad - \frac{z\, a\, \alpha_2 \Delta_E}{(1-\eta\lambda)\alpha_1 T_0 s^\beta} \frac{\partial^2 \overline{w}^*}{\partial r^2}\end{aligned} \tag{38}$$

where

$$\begin{aligned} k_1 &= \sqrt{p_1 - \sqrt{p_1^2 - 4P_2}},\ k_2 = \sqrt{p_1 + \sqrt{p_1^2 - 4P_2}}, \\ p_1 &= [D_1 s^\beta \kappa + D_2 s^\alpha \kappa + D_1 b s^{1+\beta}]/[2D_1 D_2 (bs + \kappa)], \\ P_2 &= [(1-\eta\lambda)s^{\alpha+\beta}\kappa]/[2D_1 D_2 (bs+\kappa)], \end{aligned} \tag{39}$$

and $A_1,\ A_2,\ A_3,\ A_4$ are unknown arbitrary constants that are to be determined by boundary conditions given in Eq. (21). Using Eqs. (33), (34), and (38), we can write a temperature and moisture expression in Laplace domain as

$$\begin{aligned}\overline{\theta}^* &= (D_2 k_1^2 - s^\beta)[A_1 \sin(k_1 z) + A_2 \cos(k_1 z)] + (D_2 k_2^2 - s^\beta) \\ &\quad \times [A_3 \sin(k_2 z) + A_4 \cos(k_2 z)] + \frac{z\, a \alpha_2 \Delta_E}{(1-\eta\lambda)\alpha_1 T_0 s^\beta} \frac{\partial^2 \overline{w}^*}{\partial r^2}\end{aligned} \tag{40}$$

$$\begin{aligned}\overline{\Psi}^* &= -s^\beta [A_1 \sin(k_1 z) + A_2 \cos(k_1 z)] - s^\beta [A_3 \sin(k_2 z) \\ &\quad + A_4 \cos(k_2 z)] + \frac{z\, a \alpha_2 \Delta_E}{(1-\eta\lambda)\alpha_1 T_0 s^\beta} \frac{\partial^2 \overline{w}^*}{\partial r^2}\end{aligned} \tag{41}$$

Here,

$$A_1 = \frac{-a\alpha_2 \Delta_E k_2^2 \sec[hk_1/2]}{\alpha_1 T_0 s^{2\beta} k_1 (k_1^2 - k_2^2)(1-\eta\lambda)} \frac{\partial^2 \overline{w}^*}{\partial r^2},\ A_2 = 0, \tag{42}$$

$$A_3 = \frac{a\, \alpha_2 \Delta_E k_1^2 \sec[hk_2/2]}{\alpha_1 T_0 s^{2\beta} k_2 (k_1^2 - k_2^2)(1-\eta\lambda)} \frac{\partial^2 \overline{w}^*}{\partial r^2},\ A_4 = 0 \tag{43}$$

Substitute these values of $A_1,\ A_2,\ A_3,$ and A_4 in Eqs. (38), (40), and (41), one obtains

$$\overline{F}^* = -\frac{a\alpha_2 \Delta_E [s^\beta z + f_1 \sin(k_1 z) + f_2 \sin(k_2 z)]}{(1-\eta\lambda)\alpha_1 T_0 s^{2\beta}} \frac{\partial^2 \overline{w}^*}{\partial r^2} \tag{44}$$

$$\overline{\theta}^* = \frac{a\, \alpha_2\, \Delta_E\, [z s^\beta - (D_2 k_1^2 - s^\beta) f_1 \sin(k_1 z) - (D_2 k_2^2 - s^\beta) f_2 \sin(k_2 z)]}{(1-\eta\lambda)\alpha_1 T_0 s^{2\beta}} \frac{\partial^2 \overline{w}^*}{\partial r^2} \tag{45}$$

$$\overline{\Psi}^* = \frac{a\, \alpha_2 \Delta_E\, [z - f_1 \sin(k_1 z) - f_2 \sin(k_2 z)]}{(1-\eta\lambda)\alpha_1 T_0 s^\beta} \frac{\partial^2 \overline{w}^*}{\partial r^2} \tag{46}$$

where

$$f_1 = \frac{k_2^2 \sec(ahk_1/2)}{k_1 (k_1^2 - k_2^2)},\ f_2 = \frac{k_1^2 \sec(ahk_2/2)}{k_2 (k_2^2 - k_1^2)}. \tag{47}$$

Next, to find the hygrothermal moment and deflection, take the Laplace transform of Eqs. (23) and (25), one obtains

$$\nabla_1^4 \overline{w} + \nabla_1^2 \overline{M}_T + \frac{\rho A}{EI} s^2 \overline{w} = 0 \tag{48}$$

$$\overline{M}_T = \frac{12T_0}{ah^3}\int_{-h/2}^{h/2}(\beta_1\overline{\theta} + \beta_2\lambda\overline{\Psi})\,z\,\mathrm{d}z \tag{49}$$

Using Eq. (36) above Eqs. (48) and (49) can be written as

$$\nabla_1^4\overline{w}^* + \frac{1}{a^2}\nabla_1^2\overline{M}_T^* + \frac{\rho Ac^2}{EI}s^2\overline{w}^* = 0 \tag{50}$$

$$\overline{M}_T^* = \frac{12T_0}{ah^3(s-i\Omega)}\int_{-h/2}^{h/2}(\beta_1\overline{\theta}^* + \beta_2\lambda\overline{\Psi}^*)\,z\,\mathrm{d}z \tag{51}$$

Substituting Eqs. (45) and (46) in Eq. (51), we get

$$\overline{M}_T^* = \frac{\alpha_2\,\Delta_E s^{-2\beta}(\beta_1+\beta_2)}{\alpha_1(1-\eta\lambda)(s-i\Omega)}[1+g(\Omega_1)]\frac{\partial^2\overline{w}^*}{\partial r^2} \tag{52}$$

where

$$g(\Omega_1) = \sum_{i=1}^{2}\frac{24g_i}{ki^3}\left[\frac{k_ih}{2} - \tan\left(\frac{k_ih}{2}\right)\right] \tag{53}$$

$$g_1 = \frac{k_2^2}{(k_1^2-k_2^2)}\left[\frac{\beta_1(D_2k_1^2 - s^\beta) + \beta_2\lambda s^\beta}{h^3(\beta_1+\beta_2\lambda)s^\beta}\right] \tag{54}$$

$$g_2 = \frac{k_1^2}{(k_2^2-k_1^2)}\left[\frac{\beta_1(D_2k_2^2 - s^\beta) + \beta_2\lambda s^\beta}{\overline{h}^3(\beta_1+\beta_2\lambda)s^\beta}\right] \tag{55}$$

By putting the value of hygrothermal moment from Eq. (52) in Eq. (50), we obtain the hygrothermoelastic vibration of a cylinder as,

$$\overline{w}^* = B_1\sin(qr) + B_2\cos(qr) + B_3\sin(qr) + B_4\cos(qr) \tag{56}$$

where

$$q = \left[\frac{A\rho c^2s^2}{EI(\eta\lambda-1)(s-i\Omega)}\right]^{1/4} \tag{57}$$

where the coefficients B_1, B_2, B_3,B_4 are constants. Later on, the constants will be determined by using the boundary conditions at the two ends of the cylindrical beam.

The dispersion relation between Ω and q_n is obtained as

$$\Omega = q_n^2\left\langle\frac{h^2}{12}\left\{1 + \frac{\Delta_E[1+g(\Omega)]}{1-\eta\lambda}\right\}\right\rangle^{1/2} \tag{58}$$

We neglect the corrections of higher-order terms Δ_E^2 and retain the first-order term. Additionally, in seeking an approximate solution, $g(\Omega)$ can be replaced in the square root by $g(\Omega_0)$. Now, the dispersion relation given in Eq. (58) can be written as

$$\Omega = \Omega_0\left\{1 + \frac{\Delta_E[1+g(\Omega_0)]}{2(1-\eta\lambda)}\right\} \tag{59}$$

where Ω_0 is the isothermal frequency value when $\Delta_E = 0$ in Eq. (59), then the equation can be rewritten as, $\Omega_0 = q_n^2\langle h^2/12\rangle^{1/2}$, $n = 1, 2, \ldots$

The finding, as mentioned earlier, makes it simple to separate the real and imaginary components, get the eigenfrequencies of the hygrothermoelastic cylinder, and calculate the relevant attenuation coefficients

$$\mathrm{Re}(\Omega) = \Omega_0\left\langle 1 + \frac{\Delta_E\{1+\mathrm{Re}[g(\Omega_0)]\}}{2(1-\eta\lambda)}\right\rangle \tag{60}$$

$$\mathrm{Im}(\Omega) = \frac{\Delta_E \Omega_0}{2(1-\eta\lambda)} \mathrm{Im}[g(\Omega_0)] \tag{61}$$

In other words, we expect to find that, in general, the frequencies are complex, with the real part Re(Ω) giving the new eigenfrequencies of the non-simple circular nanobeams in the presence of hygrothermoelastic coupling and the imaginary part |Im(Ω)| providing the attenuation of the vibration. The hygrothermoelastic damping in the case $\Delta_E << 1$ can be expressed in terms of the inverse quality factor given by

$$Q^{-1} = \left| 2\frac{\mathrm{Im}(\Omega)}{\mathrm{Re}(\Omega)} \right| = \frac{\Delta_E}{(1-\eta\lambda)} |\mathrm{Im}\,[g(\Omega_0)]| \tag{62}$$

The definition (62) is analogous to the definition of the Q of an electrical circuit. Here, as in the electrical analogy, Q is generally a function of frequency. The following relation is used to calculate the frequency shift caused by hygrothermoelastic damping:

$$\delta = \left| \frac{\mathrm{Re}(\Omega) - \Omega_0}{\Omega_0} \right| = \left| \frac{\Delta_E \{1 + \mathrm{Re}[g(\Omega_0)\}}{2(1-\eta\lambda)} \right| \tag{63}$$

4.2 The classical hygrothermoelastic case when $\alpha_2 = 0$

In this section, we will quickly obtain the formula for the case when both classical Fourier's and Fick's laws to frame a new model of two-temperature hygrothermoelastic diffusion theory within a fractional order system. Then, based on the governing Eqs. (16) and (17), the expression can be written in dimensionless form as

$$D_1 \left(1 + \frac{b}{\kappa}\frac{\partial}{\partial t}\right) \nabla^2 \theta = \frac{\partial^\alpha}{\partial t^\alpha}(\theta - \eta\lambda\psi),\ 0 < \alpha \leq 2 \tag{64}$$

$$D_2 \nabla^2 \psi = \frac{\partial^\beta}{\partial t^\beta}(\psi - \theta),\ 0 < \beta \leq 2 \tag{65}$$

The solution of the uncoupled equation given in Eqs. (64) and (65) is obtained by applying the Laplace transform defined in Eq. (30) and using Eqs. (33), (34), (36), which is given by,

$$\overline{\theta}^* = \frac{2(s^\beta - D_2 k_2^2)^2}{(s^\beta - D_2 k_1^2) k_1 k_2} [k_2\, \phi_1(z) + k_1\, \phi_2(z)] \tag{66}$$

$$\overline{\psi}^* = \frac{2s^\beta (s^\beta - D_2 k_2^2)}{(s^\beta - D_2 k_1^2) k_1 k_2} \left[\frac{k_2\,(s^\beta - D_2 k_2^2)}{(s^\beta - D_2 k_1^2)} \phi_1(z) + k_1 \phi_2(z) \right] \tag{67}$$

where

$$\begin{aligned} \phi_1(z) &= -\frac{\sin(k_1 z)}{\cos(k_1 h/2)} + \frac{\cos(k_1 z)}{\sin(k_1 h/2)}, \\ \phi_2(z) &= -\frac{\cos(k_2 z)}{\sin(k_2 h/2)} + \frac{\sin(k_2 z)}{\cos(k_2 h/2)}. \end{aligned} \tag{68}$$

Substitute values of temperature and moisture from Eqs. (66) and (67) in (51), we get

$$\overline{M}_T^* = \frac{T_0 (s^\beta - D_2 k_2^2)^2 g(\Omega_2)}{a\, h^3 (s^\beta - D_2 k_1^2)(s - i\,\Omega)} \tag{69}$$

where

$$g(\Omega_2) = \sum_{i=1}^{2} \frac{24 l_i}{k_i^3} \left[\frac{k_i h}{2} - \tan\left(\frac{k_i h}{2}\right) \right] \tag{70}$$

$$\begin{aligned} l_1 &= \beta_1 (s^\beta - D_2 k_2^2) + \beta_2 \lambda s^\beta \\ l_2 &= (s^\beta - D_2 k_2^2) \left[\beta_1 + \beta_2 \lambda \frac{s^\beta}{(s^\beta - D_2 k_1^2)} \right] \end{aligned} \tag{71}$$

4.3 The uncoupled case when $\eta = \lambda = 0$

If $\eta = \lambda = 0$, then, the linear relation between the water vapor concentration and the temperature disappears. In such a situation, the governing Eqs. (16) and (17) in dimensionless form can be written as,

$$D_1\left(1+\frac{b}{\kappa}\frac{\partial}{\partial t}\right)\nabla^2\theta = \frac{\partial^\alpha}{\partial t^\alpha}\left(\theta - \frac{z\,a\,\alpha_2\Delta_E}{\alpha_1 T_0}\frac{\partial^2 w}{\partial r^2}\right),\ 0<\alpha\le 2, \tag{72}$$

$$D_2\nabla^2\psi = \frac{\partial^\beta \psi}{\partial t^\beta},\ 0<\beta\le 2, \tag{73}$$

To solve Eqs. (72) and (73), apply the Laplace transform defined in Eq. (30), and using Eq. (36), and after simplification, we get the temperature and moisture as

$$\overline{\theta}^* = \frac{\alpha_2\Delta_E}{\alpha_1 T_0}\left[z - \frac{\sin(k_3 z)}{k_3\cos(ahk_3/2)}\right]\frac{\partial^2\overline{w}^*}{\partial r^2}, \tag{74}$$

$$\overline{\psi}^* = 0, \tag{75}$$

in which

$$k_3 = \sqrt{\kappa/D_1}\,s^{\alpha/2}/\sqrt{sb+\kappa}. \tag{76}$$

When heat and moisture are considered separately, it is clear that the influence of humidity is nullified. In other words, the uncoupled hygrothermoelastic model represents the pure thermoelastic model, and humidity no longer contributes.

With the help of Eqs. (51), (74), and (75), one can obtain the hygrothermal moment

$$\overline{M}_T^* = \frac{\beta_1\alpha_2\Delta_E}{a\alpha_1(s-i\Omega)}[1+g(\Omega_3)]\frac{\partial^2\overline{w}^*}{\partial r^2} \tag{77}$$

where

$$g(\Omega_3) = \frac{24}{(hk_3)^3}\left[\frac{hk_3}{2} - \tan\left(\frac{hk_3}{2}\right)\right]. \tag{78}$$

Using Eqs. (50), (69), and (77), one can obtain hygrothermoelastic vibration mode, damping, and frequency shift for the remaining cases in the form of Eqs. (56), (62), and (63), which are omitted for the sake of brevity.

5 Numerical inversion of the Laplace transform

Here, we use the Fourier sum approximation method [37], which combines real and imaginary parts in the interval (0, 2 T). In this numerical approach, any function that exists in the Laplace domain (s-domain) can be converted to a time domain (t-domain) by the following approximation formula:

$$\begin{aligned}\overline{f}(t) = (e^{ct}/T)\Bigg\langle F(c)/2 + \sum_{k=1}^{\infty}\{&\mathrm{Re}[F(c+k\pi i/T)]\cos(k\pi t/T)\\ &-\mathrm{Im}[F(c+k\pi i/T)]\sin(k\pi t/T)\}\Bigg\rangle\end{aligned} \tag{79}$$

where $s = c \pm i\varpi$, c can be any real number greater than exponential order A (i.e.$\left|\overline{f}(t)\right| \le Me^{At}$), $\mathrm{Re}[F(c+k\pi i/T)] = \int_0^\infty e^{-ct} f(t)\cos(k\pi t/T)\mathrm{d}t$, $\mathrm{Im}[F(c+k\pi i/T)] = -\int_0^\infty e^{-ct} f(t)\sin(k\pi t/T)\mathrm{d}t$, $f(t) = \overline{f}(t) - E$, and $E = \sum e^{-2ncT} f(2nT+t),$, respectively. The convergence rate is well explained in reference [37] by reducing the truncation error using suitable series transformations like the Euler Transformation and the Epsilon algorithm.

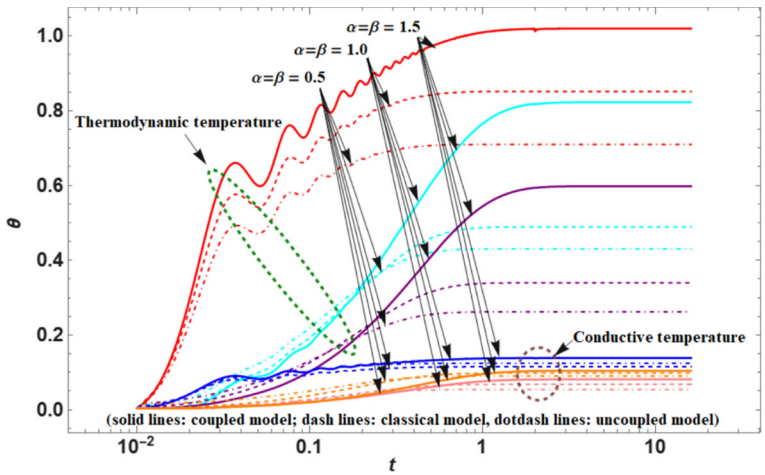

Fig. 2 Temperature distribution along t for $b = 0.2$ at different $r = 0.2, 0.5, 0.9$

6 Numerical result and discussion

This section presents a numerical calculation of the hygrothermoelastic damping of a beam for a porous composite material with the following material characteristics [1] given by,

$$\begin{gathered}\alpha_1 = 31.3 \times 10^{-6}\text{cm}/(\text{cm}^{\circ}\text{C}),\ \alpha_2 = 2.68 \times 10^{-3}\text{cm}/(\text{cm \% } H_20),\ \eta = 0.5\ \text{cm}^3{}^{\circ}C/g,\\ \lambda = 0.5\ \text{g}/(\text{cm}^3{}^{\circ}C),\ \mathfrak{D} = 2.16 \times 10^{-5}\text{m}^2/\text{s},\ D = 2.16 \times 10^{-6}\text{m}^2/\text{s},\ \omega = 0.0031\ \text{g/g}^{\circ}C,\\ \rho = 1590\,\text{kg/m}^3,\ E = 64.3\,\text{GPa},\ \nu = 0.33\end{gathered} \tag{80}$$

A beam with an aspect ratio $a/h = 10$ that experiences a quick pure heat shock (i.e., $\theta_1 = \theta_2 = 1$, $\psi_1 = \psi_2 = 0$) at both ends is used as a representation to demonstrate the transient response of temperature and moisture distribution. For the nanoscale beam, we will consider the range of beam length $a\ (1 - 100) \times 10^{-12}$ m. The original time t will be considered in the picoseconds $(1 - 100) \times 10^{-14}$ sec. The figures were prepared by using the beam length when $a = 1$, and $z = h/6$. From Fig. 2 through 6, we will discuss the temperature and moisture distribution in dimensionless form over various parameters for the coupled, classical hygrothermoelastic, and uncoupled models. For clear understanding, we draw solid lines for the coupled model, dash lines for the classical model, and dot-dash lines for the uncoupled model; the purple color curve indicates the curve at the lower value of radius ($r = 0.2$) or time ($t = 0.08$), cyan color indicates the curve at mid-value of radius ($r = 0.5$) or time ($t = 0.2$), and red color indicates the curve at the higher value of radius ($r = 0.9$) or time ($t = 0.8$). Figures 2 and 3 show the effect of hygrothermal coupling along dimensionless time t for various values of fractional order parameters α and β, for a fixed value of temperature discrepancy factor b has been depicted.

From Figs. 2 and 3, we can easily observe that the temperature distribution θ and moisture distribution ψ are significantly affected by the different values of fractional order parameter α and β for the coupled model, classical hygrothermoelastic model, and uncoupled model, respectively. As we increase the dimensionless time t, the thermodynamic temperature and conductive temperatures increase consistently, while moisture tends to decrease. It is also observed that ψ always tends to zero when time is sufficiently long, whereas θ likewise remains unchanged and does not coincide with the applied temperature. The internal heat generation within the beam is assumed to be constant; then, decreases may be due to the result of energy conversion from heat energy to strain energy as well as the hygrothermal elastic damping effect. Heat convection and radiation undoubtedly contribute to heat dissipation in real-world scenarios, but they are not considered in this study.

Figures 4 and 5 show the effect of hygrothermal coupling for the coupled model, classical hygrothermoelastic model, and uncoupled model, respectively, along r with various values of fractional order parameter α, β and for a fixed value of temperature discrepancy factor b. From Figs. 4 and 5, we can observe that as we increase the value of the fractional order parameter α and β, the temperature distribution (i.e., thermodynamic and conductive temperatures) takes higher values. In comparison, moisture takes lower values for the coupled model, classical hygrothermoelastic model, and uncoupled model, respectively, for r.

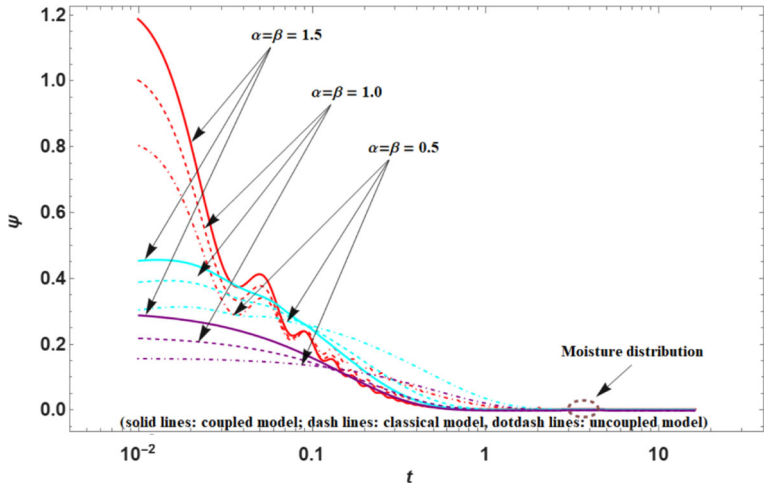

Fig. 3 Moisture distribution along t for $b = 0.2$ at different $r = 0.2, 0.5, 0.9$

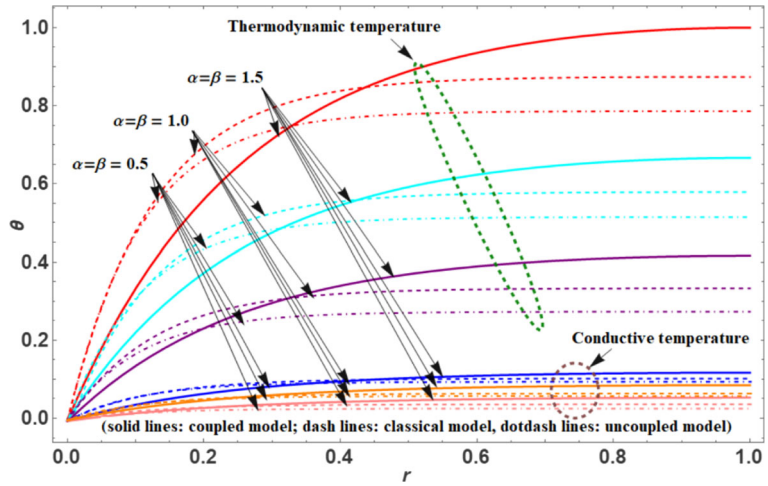

Fig. 4 Temperature distribution along r for $b = 0.2$ at different $t = 0.08, 0.2, 0.8$

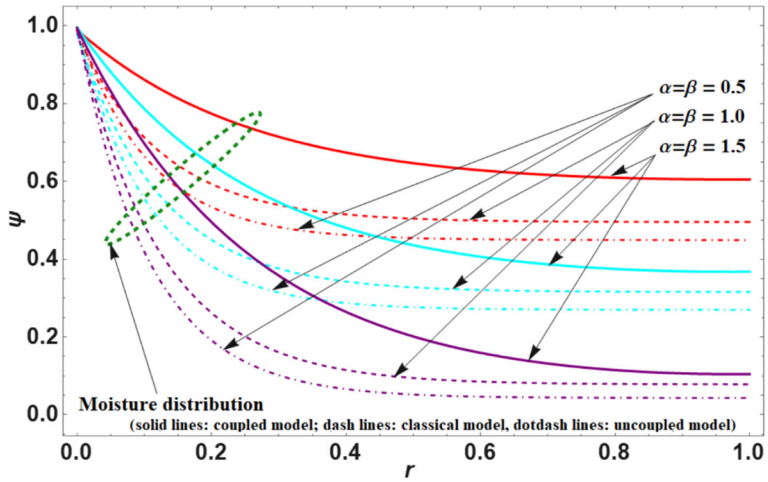

Fig. 5 Moisture distribution along r for $b = 0.2$ at different $t = 0.08, 0.2, 0.8$

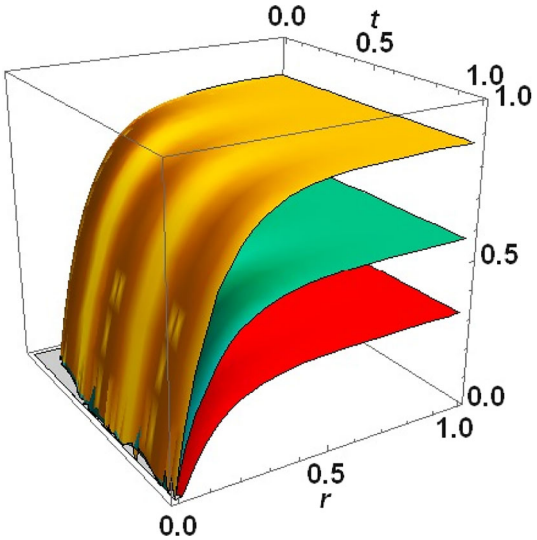

Fig. 6 Temperature distribution along r and t for various $b = 2, 1.7, 0.7$

Figure 6 shows the 3D graph of temperature distribution along r and t for various values of the temperature discrepancy factor b. When the value $b = 0$ indicates the above model has reduced to one temperature theory, whereas if $b \neq 0$, it represents two temperature theories. Temperature distribution increases with a rise in the difference of temperature value factor b. The maximum temperature occurs at the outer edge of the plate due to the available uniform sectional heat supply. When $b = 2$ and $0.5 < t < 1$, temperature graph shows sharp oscillations due to the energy conversion of heat energy to strain energy and also due to the presence of a hygrothermal damping effect. In is also learned that vapor–liquid interface cannot find a stable state, the temperature and humidity keep oscillating. At low temperatures load, evaporation only makes a small amount of vapor, and the liquid–vapor interface moves back and forth. For loads with high temperatures, the amount of vapor exceeds the system's handle, so it sometimes rushes out periodically. Thus, the mass flow rate will lead to oscillations in both of these situations. The obtained outcome is consistent with the findings reported earlier [38].

Next, only the first-order mode of a doubly clamped beam's results are calculated. The variation in hygrothermoelastic damping $Q^{-1}/\Delta E$ and frequency shift $\delta/\Delta E$ along thickness h for various values of $r = 0.2, 0.5, 0.9$ and fractional order parameter α,β with a fixed value of temperature discrepancy factor b and aspect ratio $a/h = 10$ are presented in Figs. 7 and 8 to emphasize the hygrothermoelastic coupling effects. From Fig. 7, it is clear that there are significant discrepancies in the coupled, classical, and uncoupled models for various values of α, β and found that they have distinct maximum hygrothermoelastic damping values for different values of fractional order parameters α, β. The hygrothermoelastic damping $Q^{-1}/\Delta E$ is sensitive in the range of 10^{-1} μm to 10 μm. The value of the damping $Q^{-1}/\Delta E$ steadily increases after 0.7 μm, reaches its maximum value at approximately $\overline{h} = 6$ μm, and then starts to decrease; for other thicknesses $\overline{h}$, hygrothermoelastic damping $Q^{-1}/\Delta E$ can be ignored. As we increase the value of the fractional order parameter α and β, we can observe that the value of hygrothermoelastic damping $Q^{-1}/\Delta E$ also increases with respect to thickness h for the coupled, classical, and uncoupled models.

Figure 8 shows the variations of hygrothermoelastic frequency shift $\delta/\Delta E$ in dimensionless form along thickness h for various values of $r = 0.2, 0.5, 0.9$, and fractional order parameters α and β with a fixed value of temperature discrepancy factor b and aspect ratio $a/h = 10$. From Fig. 8, one can observe that there is no impact of fractional order parameter α and β on frequency shift till 1 μm of thickness in the coupled model, classical model, and uncoupled model, while after 1 μm of thickness, there is a significant impact of fractional order parameter α and β on frequency shift for the coupled, classical, and uncoupled models and also the frequency shift $\delta/\Delta E$ has a clear difference between the coupled, classical, and uncoupled models. Between 6 μm and 14 μm of thickness, we can see the sudden picks in the graph of the coupled, classical, and uncoupled models for various values of α, β and attain maximum frequency shift pick value for the range of 6 μm to 14 μm at 10 μm of thickness. The hygrothermoelastic frequency shift $\delta/\Delta E$ starts to increase again for thickness beyond 14 μm, and we can observe the maximum variation of hygrothermoelastic frequency shift $\delta/\Delta E$ is

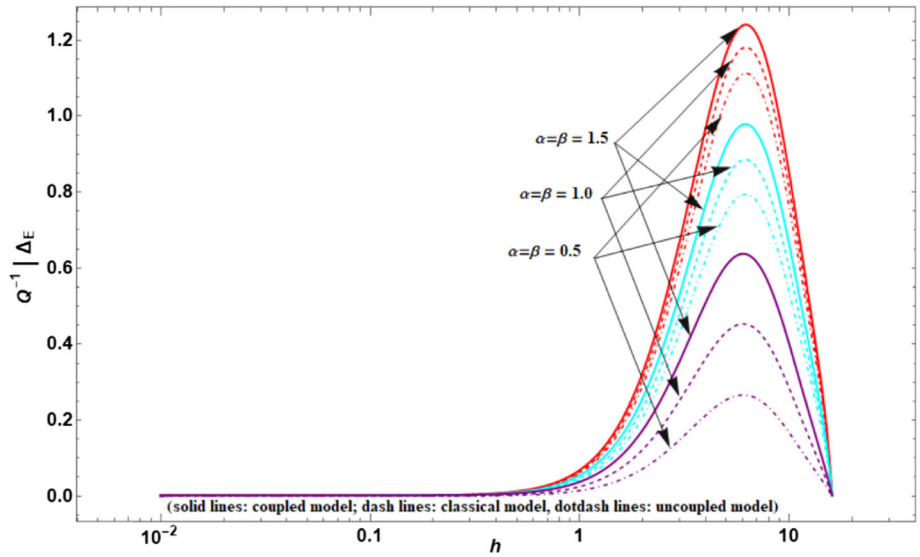

Fig. 7 Damping along thickness for $b = 0.2$, $t = 0.09$, $a/h = 10$ at $r = 0.2, 0.5, 0.9$

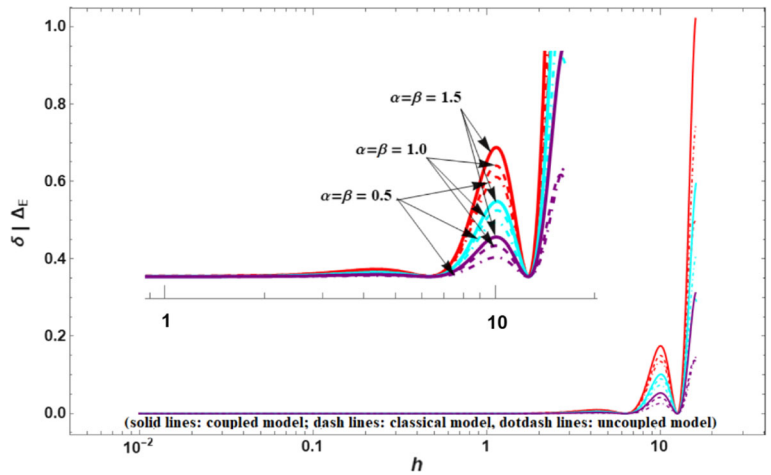

Fig. 8 Frequency shift along thickness for $b = 0.2$, $t = 0.09$, $a/h = 10$ at $r = 0.2, 0.5, 0.9$

obtained in this case for the coupled, classical, and uncoupled models for various values of fractional order parameters α, β. It is learned that it is more challenging to determine precise material damping compared to frequencies. It was discovered that damping ratios marginally increase as temperature and moisture rise. The change in damping may be masked by the measurement noise since the variation in temperature and moisture in this location is not considerable and the measurement uncertainty level for damping is very large [39]. The idea that elastic deformation is affected by moisture absorption but does not cause changes in the solid's moisture content may be the cause. It may be expected that the non-Fick effect or the time's influence will change the damping and frequency shift when absorbed moisture and elastic deformation are related to one another. There is minimal evidence of a relationship between damping and frequency shift of the beam with temperature or moisture. Thus, Figs. 7 and 8 illustrate temperature and moisture have little impact on damping and frequency shift. It is also observed that if we take various aspect ratios $a/h = 10,\ 15,\ 20,\ 25$ (or so on to say) and redraw the graph as shown in Figs. 7 and 8, then in each case, the magnitude of curves with $a/h = 15,\ 20,\ 25$ will always lie below $a/h = 10$, even though the same has not been illustrated for the sake of brevity. It is simple to compare the outcomes of the current model to earlier work [29].

7 Conclusion

In order to investigate the damping and frequency shift of an Euler–Bernoulli nanobeam, the authors of this study came up with a coupled generalized hygrothermoelastic model that included non-Fourier and non-Fick effects. An explicit formula was presented, which is used to compute the frequency shift and inverse quality factor. One can also find the closed-form solutions of hygrothermal fields in the Laplace domain. A detailed study was conducted for hygrothermoelastic damping for various aspect ratios and end constraints. We discussed how the aspect ratio and the end limitation affected the damping and frequency shift. Followings are some of the inferences that can be derived from the numerical results:

Taking into account the presence of moisture results in more damping as a consequence of increased energy dissipation.

- The frequency shift and damping are affected by the time period it takes for heat flux to relax. The damping and frequency shift are almost entirely unaffected by the time it takes for moisture flux to relax.
- The damping and frequency shift are notably sensitive to the non-Fourier effect for beams with thicknesses of 10^{-1} μm to 10 μm. Still, they are almost disrespectful to the non-Fick effect.
- The influence of the isothermal dimensionless fundamental frequencies on the frequency shift and damping is explored. Different end constraints or aspect ratios correspond to distinct isothermal frequencies, resulting in distinct frequency shifts and damping.
- The response history and distribution of the hygrothermal fields are significantly impacted by the linked non-Fourier and non-Fick effects, which have a non-Fourier effect. Even without heat transfer via convection and radiation to the surrounding environment, a temperature drop can occur due to hygrothermoelastic damping, leading to energy loss.

Declarations

Conflict of interest On behalf of all authors, I state that there is no conflict of interest. None of the authors of this study has any financial or personal connections to any individuals or groups that would unfairly prejudice or affect the paper's content.

References

1. Sih, G.C., Michopoulos, J.G., Chou, S.C. (Eds.): Hygrothermoelasticity. Springer Netherlands (1986). https://doi.org/10.1007/978-94-011-3734-8_6
2. Chang, W.J., Weng, C.I.: An analytical solution to coupled heat and moisture diffusion transfer in porous materials. Int. J. Heat Mass Transf. **43**(19), 3621–3632 (2000). https://doi.org/10.1016/S0017-9310(00)00003-X
3. Benkhedda, A., Tounsi, A., Addabedia, E.A.: Effect of temperature and humidity on transient hygrothermal stresses during moisture desorption in laminated composite plates. Compos. Struct. **82**(4), 629–635 (2008). https://doi.org/10.1016/j.compstruct.2007.04.013
4. Nguyen, T.K., Nguyen, B.D., Vo, T.P., Thai, H.T.: Hygro-thermal effects on vibration and thermal buckling behaviours of functionally graded beams. Compos. Struct. **176**, 1050–1060 (2017). https://doi.org/10.1016/j.compstruct.2017.06.036
5. Zenkour, A.M.: Bending of thin rectangular plates with variable-thickness in a hygrothermal environment. Thin-Walled Struct. **123**, 333–340 (2018). https://doi.org/10.1016/j.tws.2017.11.038
6. Tang, Y., Ding, Q.: Nonlinear vibration analysis of a bi-directional functionally graded beam under hygro-thermal loads. Compos. Struct. **225**, 111076 (2019). https://doi.org/10.1016/j.compstruct.2019.111076
7. Bhoyar, S., Varghese, V., Khalsa, L.: Hygrothermoelastic response in the bending analysis of elliptic plate due to hygrothermal loading. J. Therm. Stress. **43**(3), 372–400 (2020). https://doi.org/10.1080/01495739.2019.1711477
8. Jan, M.T., Ahmad, F., Hamid, N.H.B., Khir, M.H.B.M., Shoaib, M., Ashraf, K.: Experimental investigation of temperature and relative humidity effects on resonance frequency and quality factor of CMOS-MEMS paddle resonator. Microelectron. Reliab. **63**, 82–89 (2016). https://doi.org/10.1016/j.microrel.2016.05.007
9. Eichler, A., Moser, J., Chaste, J., Zdrojek, M., Wilson-Rae, I., Bachtold, A.: Nonlinear damping in mechanical resonators made from carbon nanotubes and graphene. Nat. Nanotechnol. **6**(6), 339–342 (2011). https://doi.org/10.1038/nnano.2011.71
10. Ebrahimi, F., Barati, M.R.: Hygrothermal effects on static stability of embedded single-layer graphene sheets based on nonlocal strain gradient elasticity theory. J. Therm. Stress. **42**(12), 1535–1550 (2019). https://doi.org/10.1080/01495739.2019.1662352
11. Lord, H.W., Shulman, Y.: A generalized dynamical theory of thermoelasticity. J. Mech. Phys. Solids **15**(5), 299–309 (1967). https://doi.org/10.1016/0022-5096(68)90024-5
12. Tzou, D.Y.: A unified field approach for heat conduction from macro- to micro-scales. J. Heat Transf. **117**(1), 8–16 (1995). https://doi.org/10.1115/1.2822329

13. Povstenko, Y. Fractional Thermoelasticity, New York:Springer (2015). https://doi.org/10.1007/978-3-319-15335-3
14. Sun, Y., Fang, D., Soh, A.K.: Thermoelastic damping in micro-beam resonators. Int. J. Solids Struct. **43**(10), 3213–3229 (2006). https://doi.org/10.1016/j.ijsolstr.2005.08.011
15. Kakhki, E.K., Hosseini, S.M., Tahani, M.: An analytical solution for thermoelastic damping in a micro-beam based on generalized theory of thermoelasticity and modified couple stress theory. Appl. Math. model. **40**(4), 3164–3174 (2016). https://doi.org/10.1016/j.apm.2015.10.019
16. Youssef, H.M., El-Bary, A.A., Al-Lehaibi, E.A.N.: Characterization of the quality factor due to the static prestress in classical Caputo and Caputo-Fabrizio fractional thermoelastic silicon microbeam. Polymers **13**(1), 27 (2020). https://doi.org/10.3390/polym13010027
17. Hughes, J.E. Jr., Di Ventra, M, Evoy, S.: Introduction to nanoscale science and technology. *Nanostructure Science and Technology*. Berlin: Springer. (2004). https://doi.org/10.1007/b119185
18. Elsibai, K.A., Youssef, H.M.: State-space approach to vibration of gold nanobeam induced by ramp type heating without energy dissipation in femtoseconds scale. J. Therm. Stress. **34**(3), 244–263 (2011). https://doi.org/10.1080/01495739.2010.545737
19. Zhou, H., Li, P.: Dual-phase-lagging thermoelastic damping and frequency shift of micro/nano-ring resonators with rectangular cross-section. Thin-Walled Struct. **159**, 107309 (2021). https://doi.org/10.1016/j.tws.2020.107309
20. Wang, Y.W., Zhang, X.Y., Li, X.F.: Thermoelastic damping in a micro-beam based on the memory-dependent generalized thermoelasticity. Wave Random Complex **32**(6), 2812–2829 (2022). https://doi.org/10.1080/17455030.2020.1865590
21. Shaw, S., Othman, M.I.A.: Computational analysis on the influence of damping in solid body deformation during thermoelastic mass diffusion. Wave Random Complex **32**(2), 597–617 (2022). https://doi.org/10.1080/17455030.2020.1788747
22. Ezzat, M.A., Othman, M.I., Smaan, A.A.: State space approach to two-dimensional electromagneto–thermoelastic problem with two relaxation times. Int. J. Engrg. Sci. **39**(12), 1383–1404 (2001). https://doi.org/10.1016/S0020-7225(00)00095-1
23. El-Karamany, A.S., Ezzat, M.A.: Thermoelastic diffusion with memory-dependent derivative. J. Therm. Stress. **39**(9), 1035–1050 (2016). https://doi.org/10.1080/01495739.2016.1192847
24. Hosseini, S.M., Rad, M.H.G.: Application of meshless local integral equations for two-dimensional transient coupled hygrothermoelasticity analysis: Moisture and thermoelastic wave propagations under shock loading. J. Therm. Stress. **40**(1), 40–54 (2016). https://doi.org/10.1080/01495739.2016.1224134
25. Peng, Y., Zhang, X.Y., Li, X.F.: Effect of phase lags of moisture–heat flow on the hygrothermoelastic field of hollow cylinders with convective surfaces. Mech. Based Des. Struct. Mach. (2021). https://doi.org/10.1080/15397734.2021.1914654
26. Xue, Z., Tian, X., Liu, J.: Non-classical hygrothermal fracture behavior of a hollow cylinder with a circumferential crack. Eng. Fract. Mech. **224**, 106805 (2020). https://doi.org/10.1016/j.engfracmech.2019.106805
27. Zhang, X.Y., Li, X.F.: Transient response of a hygrothermoelastic cylinder based on fractional diffusion wave theory. J. Therm. Stress. **40**(12), 1575–1594 (2017). https://doi.org/10.1080/01495739.2017.1344111
28. Zhang, X.Y., Li, X.F.: Transient response of hygrothermoelastic field in an elastic plate with an edge crack. Z. Angew. Math. Phys. **100**(9), e202000005 (2020). https://doi.org/10.1002/zamm.202000005
29. Zhang, X.Y., Li, X.F.: Hygrothermoelastic damping of beam resonators with non-Fourier and non-Fick effects. Thin Wall Struct. **168**, 108283 (2021). https://doi.org/10.1016/j.tws.2021.108283
30. Chang, W.J., Chen, T.C., Weng, C.I.: Transient hygrothermal stresses in an infinitely long annular cylinder: coupling of heat and moisture. J. Therm. Stress. **14**, 439–454 (1991). https://doi.org/10.1080/01495239108927078
31. Povstenko, Y.: Non-axisymmetric solutions to time-fractional diffusion-wave equation in an infinite cylinder. Fract. Calc. Appl. Anal. **14**, 418–435 (2011)
32. Kilbas, A.A.A., Srivastava, H.M., Trujillo, J.J.: Theory and Applications of Fractional Differential Equations. Elsevier Science Limited, Amsterdam (2006)
33. Chen, P.J., Gurtin, M.E.: On a theory of heat conduction involving two temperatures. Z. Angew. Math. Phys. **19**, 559–577 (1968). https://doi.org/10.1007/BF01594969
34. Chen, P.J., Gurtin, M.E., Willams, W.O.: On the thermodynamics of non-simple elastic material with two temperatures. Z. Angew. Math. Phys. **20**, 107–112 (1969). https://doi.org/10.1007/BF01591120
35. Lifshitz, R., Roukes, M.L.: Thermoelastic damping in micro- and nanomechanical systems. Phys. Rev. B **56**(8), 5100–5109 (2000). https://doi.org/10.1103/PhysRevB.56.5100
36. Meirovitch, L.: *Principles and Techniques of Vibrations*, Englewood Cliffs, NJ: Prentice-Hall Inc, International Edition (1997).
37. Crump, K.S.: Numerical inversion of Laplace transforms using a Fourier-series approximation. J. ACM **23**(1), 89–96 (1976)
38. Zenkour, A.M., Abouelregal, A.E.: Non-simple magneto-thermoelastic solid cylinder with variable thermal conductivity due to harmonically varying heat. Earthq. Struct. **10**(3), 681–697 (2016). https://doi.org/10.12989/eas.2016.10.3.681
39. Zhou, G.-D., Yi, T.-H.: A summary review of correlations between temperatures and vibration properties of long-span bridges. Math. Probl. Eng. **2014**, 638209 (2014). https://doi.org/10.1155/2014/638209

Terms and Conditions

Springer Nature journal content, brought to you courtesy of Springer Nature Customer Service Center GmbH (“Springer Nature”).
Springer Nature supports a reasonable amount of sharing of research papers by authors, subscribers and authorised users (“Users”), for small-scale personal, non-commercial use provided that all copyright, trade and service marks and other proprietary notices are maintained. By accessing, sharing, receiving or otherwise using the Springer Nature journal content you agree to these terms of use (“Terms”). For these purposes, Springer Nature considers academic use (by researchers and students) to be non-commercial.
These Terms are supplementary and will apply in addition to any applicable website terms and conditions, a relevant site licence or a personal subscription. These Terms will prevail over any conflict or ambiguity with regards to the relevant terms, a site licence or a personal subscription (to the extent of the conflict or ambiguity only). For Creative Commons-licensed articles, the terms of the Creative Commons license used will apply.
We collect and use personal data to provide access to the Springer Nature journal content. We may also use these personal data internally within ResearchGate and Springer Nature and as agreed share it, in an anonymised way, for purposes of tracking, analysis and reporting. We will not otherwise disclose your personal data outside the ResearchGate or the Springer Nature group of companies unless we have your permission as detailed in the Privacy Policy.
While Users may use the Springer Nature journal content for small scale, personal non-commercial use, it is important to note that Users may not:

1. use such content for the purpose of providing other users with access on a regular or large scale basis or as a means to circumvent access control;
2. use such content where to do so would be considered a criminal or statutory offence in any jurisdiction, or gives rise to civil liability, or is otherwise unlawful;
3. falsely or misleadingly imply or suggest endorsement, approval , sponsorship, or association unless explicitly agreed to by Springer Nature in writing;
4. use bots or other automated methods to access the content or redirect messages
5. override any security feature or exclusionary protocol; or
6. share the content in order to create substitute for Springer Nature products or services or a systematic database of Springer Nature journal content.

In line with the restriction against commercial use, Springer Nature does not permit the creation of a product or service that creates revenue, royalties, rent or income from our content or its inclusion as part of a paid for service or for other commercial gain. Springer Nature journal content cannot be used for inter-library loans and librarians may not upload Springer Nature journal content on a large scale into their, or any other, institutional repository.
These terms of use are reviewed regularly and may be amended at any time. Springer Nature is not obligated to publish any information or content on this website and may remove it or features or functionality at our sole discretion, at any time with or without notice. Springer Nature may revoke this licence to you at any time and remove access to any copies of the Springer Nature journal content which have been saved.
To the fullest extent permitted by law, Springer Nature makes no warranties, representations or guarantees to Users, either express or implied with respect to the Springer nature journal content and all parties disclaim and waive any implied warranties or warranties imposed by law, including merchantability or fitness for any particular purpose.
Please note that these rights do not automatically extend to content, data or other material published by Springer Nature that may be licensed from third parties.
If you would like to use or distribute our Springer Nature journal content to a wider audience or on a regular basis or in any other manner not expressly permitted by these Terms, please contact Springer Nature at

onlineservice@springernature.com